Seismic structure of the upper mantle beneath the Philippine Sea from seafloor and land observation: Implications for mantle convection and magma genesis in the Izu–Bonin–Mariana subduction zone

Takehi Isse [a,*], Hajime Shiobara [a], Yoshihiko Tamura [b], Daisuke Suetsugu [b], Kazunori Yoshizawa [c,1], Hiroko Sugioka [b], Aki Ito [b], Toshihiko Kanazawa [a], Masanao Shinohara [a], Kimihiro Mochizuki [a], Eichiro Araki [d], Kazuo Nakahigashi [a], Hitoshi Kawakatsu [a], Azusa Shito [b], Yoshio Fukao [b], Osamu Ishizuka [e], James B. Gill [f]

[a] Earthquake Research Institute, University of Tokyo, 1-1-1, Yayoi, Bunkyo-ku, Tokyo 113-0032, Japan
[b] Institute for Research on Earth Evolution (IFREE), Japan Agency for Marine-Earth Science and Technology (JAMSTEC), Yokosuka 237-0061, Japan
[c] Department of Natural History Sciences, Faculty of Science, Hokkaido University, Sapporo 060-0810, Japan
[d] Department of Oceanfloor Network System for Earthquakes and Tsunamis (DONET), Japan Agency for Marine-Earth Science and Technology (JAMSTEC), Yokosuka 237-0061, Japan
[e] Institute of Geoscience, Geological Survey of Japan/AIST, Central 7, 1-1-1 Higashi, Tsukuba, Ibaraki 305-8567, Japan
[f] Earth and Planetary Sciences Department, University of California, Santa Cruz CA 95064, USA

ARTICLE INFO

ABSTRACT

We have determined the three-dimensional shear wave speed structure of the upper mantle in and around the Philippine Sea region using seismograms recorded by dense land-based and long-term broadband ocean bottom seismographic stations. We used a surface wave tomography technique in which multimode phase speeds are measured and inverted for a 3-D shear wave speed structure by incorporating the effects of a finite frequency and ray bending. The new ocean bottom data provided us with improved spatial resolution (~300 km) in the Philippine Sea region. In the upper 120 km, the shear wave speed structure is well correlated with seafloor age. At depths greater than 160 km, fast anomalies of the subducting Pacific Plate are clearly defined. We also found slow speed anomalies beneath the Kyushu–Palau ridge at depths greater than 120 km. Along the Izu–Bonin(Ogasawara)–Mariana arc, we have detected three separate slow anomalies in the mantle wedge at depths shallower than 100 km beneath the back arc. Each anomaly has a width of ~500 km. Moreover, these three anomalies have a close relationship with the three groups of frontal and rear arc volcanoes having distinct Sr, Nd, and Pb isotope ratios. We suggest that each of the anomalies is a site of large-scale flow of upper mantle into the mantle wedge, and that each already contains a component from the adjacent subducting slab.

© 2008 Elsevier B.V. All rights reserved.

1. Introduction

The upper mantle structure beneath the Philippine Sea Plate has been extensively studied using surface waves (Kanamori and Abe, 1968; Oda and Senna, 1994). Lebedev et al. (1997), and Nakamura and Shibutani (1998) performed regional surface wave tomography to obtain 3-D shear wave speed structure models beneath the Philippine Sea. Gorbatov and Kennett (2003) obtained body wave tomography images of the Philippine Sea using P and S travel times with a joint inversion in terms of bulk-sound and shear wave speed variations in the mantle. However, the lack of seismic stations and earthquakes in the mid Philippine Sea limited the lateral resolution of the upper mantle in all of these previous models, and made it difficult to reduce artifacts caused by structures outside the Philippine Sea.

Since the 1990s, a dense broadband seismic network called F-net (formerly called FREESIA) has been deployed across Japan by the National Institute for Earth Science and Disaster Prevention (Fukuyama et al., 1996) and a broadband seismic network has been deployed in the western Pacific Ocean by the Ocean Hemisphere network Project (OHP) (Fukao et al., 2001). As a part of the OHP, long-term broadband ocean bottom seismometers (called BBOBS hereafter) have been developed and a linear array of BBOBSs was operated in the Philippine Sea and the northwestern Pacific Ocean between 1999 and 2000 (Kanazawa et al., 2001; Shiobara et al., 2001). The BBOBS data have improved the spatial resolution substantially within the Philippine Sea region (Isse et al., 2004, 2006). Isse et al. (2004) showed that the quality of BBOBS equiped with PMD sensors with a flat frequency response at periods between 0.05 and 30 s was comparable with that of land stations in the periods between 20 and 100 s, indicating that the BBOBSs were useful for surface wave studies. Isse et al. (2006) obtained

the three-dimensional shear wave speed structure of the upper mantle beneath the Philippine Sea and the surrounding region from seismograms recorded by land-based and long-term broadband ocean bottom seismographic stations. The model showed that the shear wave speed structure in the upper 120 km was well correlated with the age of the provinces, and that the pattern was dominated by fast anomalies in the subducted Pacific Plate and two slow anomalies to the south of the Daito ridge and in the southernmost part of the Philippine Sea at depths greater than 160 km. Although the spatial resolution was improved using BBOBSs data, it was not good enough to resolve finer scale differences within the region.

A new three-year project using 12–16 BBOBSs started in 2005 (Shiobara et al., 2006). It is a part of the Stagnant Slab Project that started in 2004 to study the upper mantle, the mantle transition zone, and the lower mantle in an interdisciplinary manner. The BBOBS data are planned to be recovered every year and the first and second one-year-long data records were successfully recovered in 2006 and 2007, respectively. In this study, we present a first report of the three-dimensional shear wave speed structure beneath the Philippine Sea obtained from the BBOBS observation of the Stagnant Slab Project. The new BBOBS data, along with the increased number of events used, enable us to obtain better spatial resolution compared with that in previous studies and to discuss the tectonic evolution of the Philippine Sea.

2. Geological evolution of the Philippine Sea region

The Philippine Sea region consists of several basins, troughs and ridges with various seafloor ages (Fig. 1a). It separates the Pacific, Australian and Eurasian plates, is surrounded by subduction zones. Its evolution has been closely linked to that of the Izu–Bonin (Ogasawara)–Mariana (called IBM hereafter) arc system (Hall, 2002). The IBM arc system extends 2800 km from the Izu Peninsula to Guam Island. IBM is a juvenile intra-oceanic arc system characterized by a well-developed, low-velocity middle crust with P-wave velocities of 6.0–6.5 km/s of intermediate composition (Suyehiro et al., 1996; Takahashi et al., 2007; Kodaira et al., 2007a,b), which is typical of many intra-oceanic arcs. The Izu–Bonin oceanic arc has erupted a large volume of silicic magma, comparable to the volume of basalt and basaltic andesite (Gill et al., 1994; Tamura and Tatsumi, 2002), which is a matter of considerable interest and debate (e.g., Shukuno et al., 2006). This system is uniquely suited to the study of arc crustal evolution: therefore, the Philippine Sea Plate is clearly of great importance for the evolution of both IBM arc crust and mantle.

The IBM subduction zone began as part of a hemispheric-scale foundering of old, dense lithosphere in the Western Pacific about 50 Ma (Bloomer et al., 1995; Stern, 2004), perhaps aided by reorganization of plate boundaries throughout the western Pacific (Hall et al., 2003). Initial (50–43 Ma) and first arc (42–25 Ma)
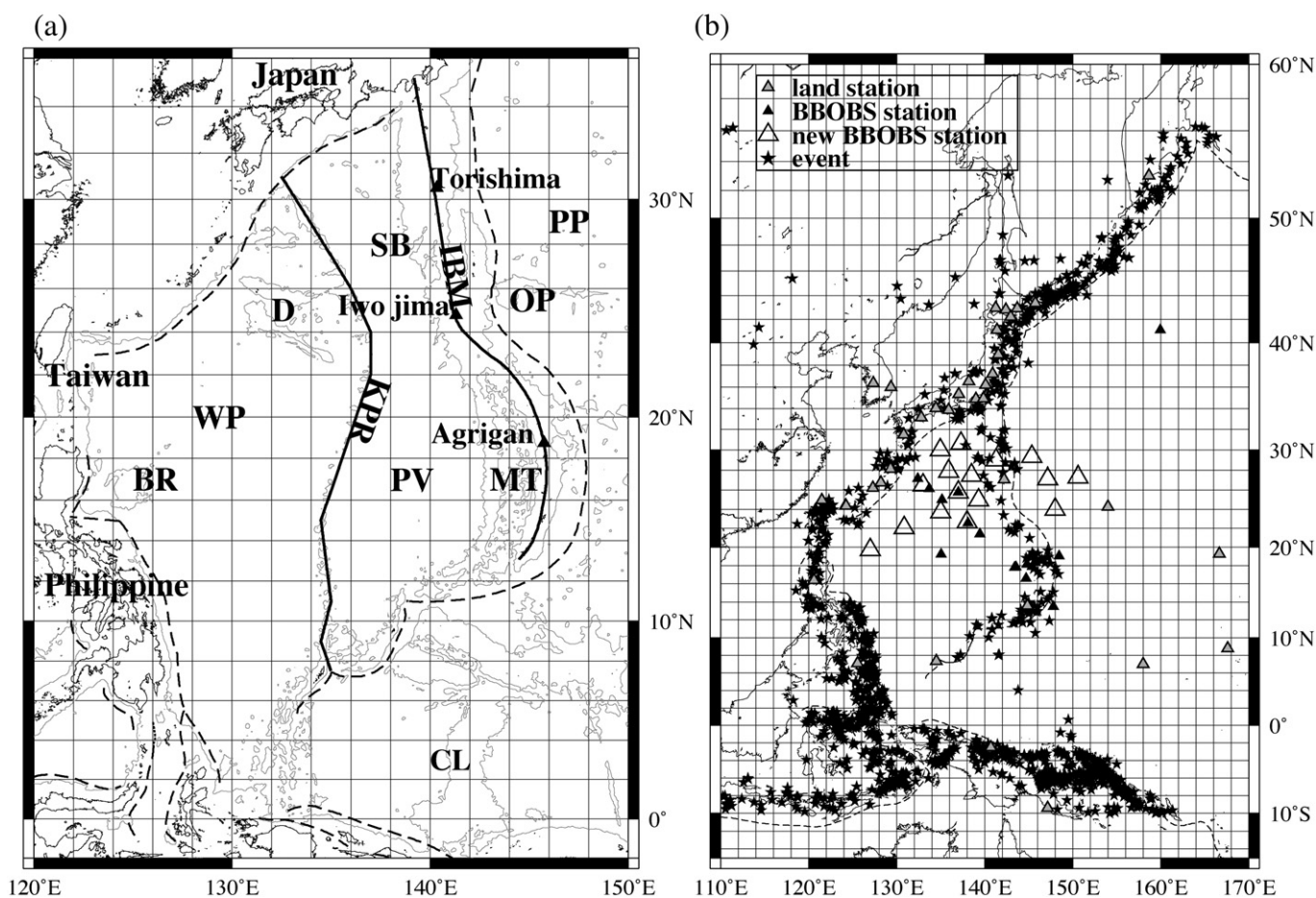

Fig. 1. (a) Tectonic features of the Philippine Sea. A gray contour indicates the bathymetry at depth of 3500 m. The broken lines indicate the plate boundary of the Philippine Sea plate, trenches and troughs. Letters represent marginal basins and tectonic features as follows in alphabetical order. Formation ages in parentheses. BR, Benham Rise (49–36 Ma); D, Amami Plateau, Oki–Daito and Daito ridges (Cretaceous–Eocene); CL, Caroline Plate (2–40 Ma); IBM, Izu–Bonin–Mariana arc (50–0 Ma); KPR, Kyushu–Palau ridge (50–25 Ma); MT, Mariana trough (7–0 Ma);OP, Ogasawara plateau (Cretaceous); PP, Pacific Plate (~150 Ma); PV, Parece–Vela basin (30–15 Ma); SB, Shikoku basin (25–15 Ma); WP, West Philippine basin (50–35 Ma). The old Pacific Plate (PP) subducts beneath the active IBM arc. KPR marks the rifted western edge of the initial IBM arc system that was subsequently separated by back-arc spreading in the Shikoku Basin (SB) and Parece Vela Basin (PV). (b) Geographical distributions of events and stations used in this study. The gray triangles indicate permanent broadband seismological stations and the black triangles indicate BBOBS stations, which we used in the previous studies. The open triangles indicate new BBOBS stations we added in this study. The solid stars indicate earthquakes used in this study.

volcanism (Taylor, 1992; Ishizuka et al., 2006) was accompanied until at least 33 Ma by spreading along the WNW–ESE (present co-ordinates) trending Central Basin Fault in the West Philippine Sea, which produced a large part of the West Philippine Basin (Deschamps and Lallemand, 2002; Taylor and Goodliffe, 2004). The West Philippine Basin (WPB) can be divided into three regions according to age and character: (1) the Central Basin area, which is clearly formed by seafloor spreading from the Central Basin Fault between 49 and 33 Ma (Taylor and Goodliffe, 2004); (2) the section north of the Oki–Daito escarpment that has a distinct spreading fabric and includes the Oki–Daito and Daito Ridges and Amami Plateau, that have island-arc lithologies of Eocene to Cretaceous age (Hickey-Vargas et al., 2006); and (3) the Benham Rise, which is a large (40 000 km^3) feature derived from a mantle plume or hotspot from 49 Ma to 36 Ma (Hickey-Vargas, 1998).

About 30 Ma, back-arc basins began to form behind the IBM arc. Spreading of the back-arc basins began in the south forming the Parece Vela Basin, and then propagated north and south. Spreading in the northernmost IBM began about 25 Ma and propagated south to form the Shikoku Basin (Okino et al., 1999). The Shikoku Basin and Parece Vela Basin spreading systems met about 20 Ma, stranding the Eocene–Oligocene Kyushu–Palau ridge (KPR) (Malyarenko and Leli-kov, 1995) as a remnant arc.

The seafloor spreading of the Mariana Trough started at about 6 Ma (Hussong and Uyeda, 1981). Spreading has not yet begun behind the Izu arc, but a series of narrow grabens, a few tens of kilometers wide, rift the Izu–Bonin arc adjacent to the active volcanic front edifices between 27° and 34°N.

The upper mantle structure beneath the Philippine Sea Plate might reflect this complex evolutionary history together with lateral variations caused by modern subduction. The age of the Western Pacific seafloor, which subducts beneath the Philippine Sea Plate, has been inferred from magnetic anomalies and confirmed by drilling. The cold Pacific Plate (130–162 Ma) subducts at 30–60 mm/yr beneath the IBM arc (Seno et al., 1993). Could the resulting mantle convection and thermal structure be uniform under the entire IBM arc, which stretches over 2800 km?

3. IBM subduction factory and data from arc volcanoes

Stern et al. (2003) presented an excellent overview of the IBM subduction factory. The magmatic front lies about 150 km above the Wadati–Benioff zone (Anglin and Fouch, 2005), with no systematic differences along the IBM arc system. Both submarine and subaerial volcanoes define the IBM magmatic front. IBM lavas from along the magmatic front of the arc show a wide range of compositions. Low-K suites characterize the Izu and most of the Bonin segments as far south as 25°N, a medium-K suite typifies most of the Mariana segment (as far north as 23°N), and a largely shoshonitic province is found between the Bonin and Mariana segment (23–25°N). Interestingly, this subdivision roughly correlates with the upper mantle structure of the IBM arc mantle wedge presented below. The Mariana segment has been subdivided into the Northern Seamount Province (NSP), Central Island Province (CIP) and Southern Seamount Province (SSP) (Bloomer et al., 1989).

We have complied isotope analyses from arc front and rear arc volcanoes in order to investigate the relationships between upper mantle structure and the isotope ratios of lavas. Rear arc lavas are from the Sumisu Rift and the Mariana Trough. Magmas at the volcanic front are rich in fluid-mobile recycled slab components that swamp the mantle below the volcanic front. This is less true in the rear arc where the diminished slab signature allows the geochemical signature of the mantle source to be tracked more easily. Extension-related suites (Mariana Trough and N. Izu rifts), and cross-chain volcanoes are both rear arc volcanoes in the sense that they show fewer effects of fluid-mobile recycled slab components. These isotopic ratios cannot be affected by crystal fractionation of magmas and/or the different degrees of partial melting of the source mantle. Contamination by old crustal rocks can change these values; however, the effect would be minimal in an oceanic arc such as IBM. Thus, these isotope ratios are characteristic of the subduction-modified mantle sources.

4. Seismic data and method

We used broadband vertical component seismograms recorded by stations in a latitudinal range from 10°S to 57°N, and a longitudinal range from 110°E to 168°E. The events we analyzed occurred in the same region since 1990 with magnitudes greater than 5.5 (Mw or Mb). Fig. 1b shows the locations of events and seismic stations that we used to obtain the three-dimensional shear wave speed structures. The number of events we used was 1399. The locations of stations used in this study are listed in Table S1. Fig. 1b shows that the distribution of seismic stations in the northern part of the Philippine Sea plate is denser than that in the previous studies.

We employed the three-stage inversion method developed by Kennett and Yoshizawa (2002) and Yoshizawa and Kennett (2004) and used by Isse et al. (2006). The method consists of three independent stages: (1) measurement of path-specific multimode phase speed dispersion; (2) two-dimensional mapping of phase speed for each mode and period by incorporating the effects of finite frequency and ray bending; and (3) inversion of multimode phase dispersion at each grid for a three-dimensional shear wave speed model (Yoshizawa and Kennett, 2004). Details of this method are given in these previous studies (Yoshizawa and Kennett, 2004; Isse et al., 2006); we explain it briefly below.

We measured the phase speeds of the fundamental and first three higher modes of Rayleigh waves by a fully nonlinear waveform inversion method (Yoshizawa and Kennett, 2002a). In this inversion method, the neighborhood algorithm (Sambridge, 1999) is adopted as a global optimizer that explores the model space to find a model with the best fit to the recorded seismograms. In total, 3000 models were generated for each path and the best-fit 1-D model was obtained from these models. The multimode phase speeds were computed from the 1-D model using normal mode theory (Takeuchi and Saito, 1972) and are regarded as the path-averaged phase speeds of each event-station pair. The standard errors of each dispersion curve were estimated from the standard deviations of the best 1000 trials among all the generated models. We used the events whose magnitudes was greater than 5.7 (Mb or Mw) for the fundamental mode and 5.5 for the higher mode. For the first higher mode, we used events whose depths were greater than 100 km. We used the data whose epicentral distance was greater than 14° to separate the higher modes from the fundamental mode. The cross-correlation between observed and synthetic data with a group velocity filter between 3.3 and 4.3 km/s was better than 0.9. We obtained 6793 phase speed dispersion curves for the fundamental mode at periods between 40 and 167 s, and 566 for the first higher mode, 1202 for the second higher mode, and 1226 for the third higher mode at periods between 40 and 120 s.

To make the ray density uniform, we clustered events observed at the same station within a cluster radius of 100 km and averaged the obtained phase speed for the clustered events. We treated the average phase speed as a path-average phase speed along a ray from the center of the cluster to the station. The number of path-averaged phase speed dispersion curves of fundamental and first three higher modes of Rayleigh wave after the clustering process was 3413, 419, 847, and 819, respectively, which is about 2.5–8 times higher than those in Isse et al. (2006). The increase in the data is mainly caused by the increased number of events used. The number of phase speed dispersion curves recorded by all BBOBSs was 643, 37, 78, and 41 for the fundamental and the first three higher modes, respectively. The estimated errors were less than 1.1% for all the path-averaged phase speed dispersion curves.
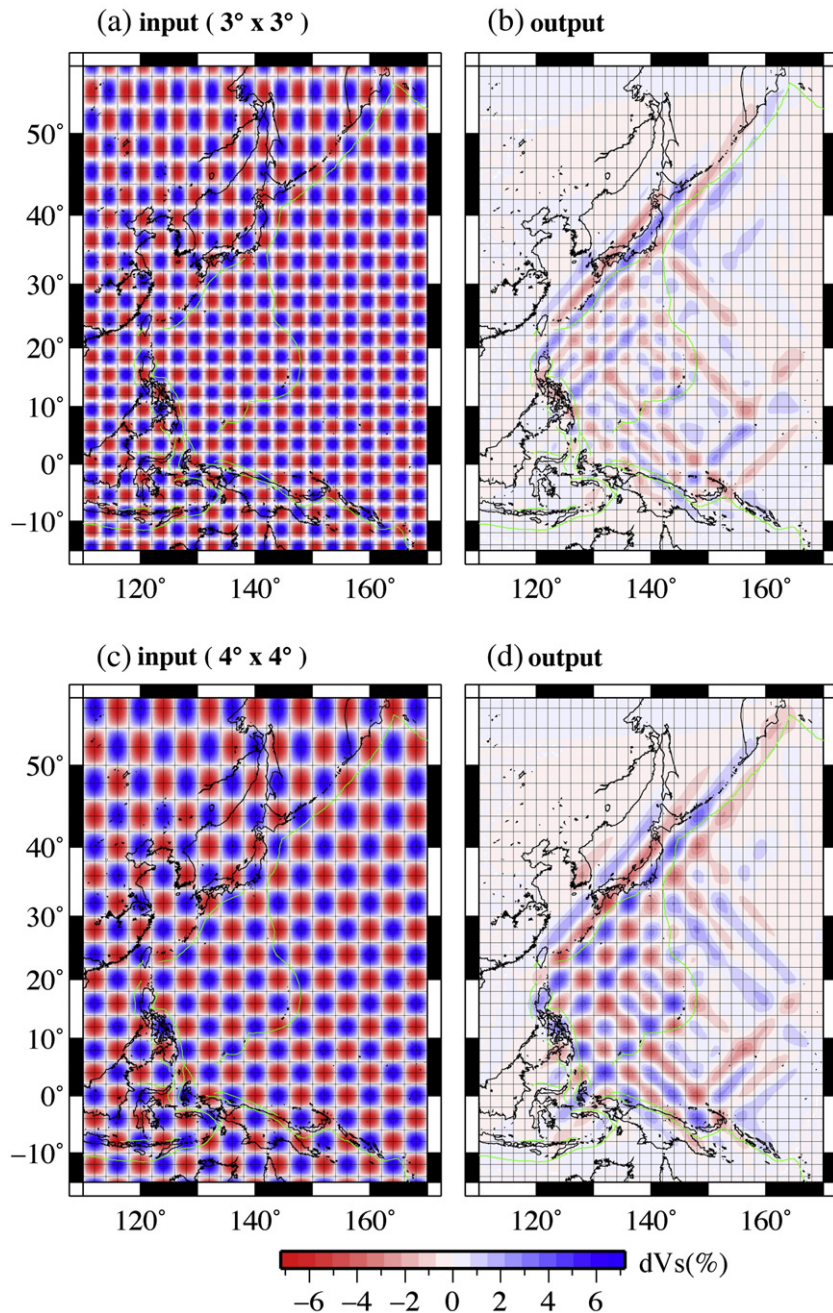
Fig. 2. Checkerboard resolution test results for the fundamental mode of 42 s with different cell sizes: (a, b) 3×3° and (c, d) 4×4°. The amplitude of the anomalies is 6%. From the left to right, input checkerboard models (a, c), and the output models recovered from all of the synthetic data (b, d).

In the second stage, we inverted the path-averaged multimode phase speeds to 2-D phase speed maps of each mode as a function of the frequency. It is this stage that considers the finite frequency effect and the ray path deviation from a great circle. The Fresnel area ray tracing technique (Yoshizawa and Kennett, 2002b) was used for tracing rays and calculating the width of the influence zone around the surface wave path at finite frequencies. A spherical B-spline function was defined at the center of a geographic cell as the basis function for expanding the phase speed perturbations. We inverted the path-averaged phase speed dispersion curves obtained above for the 2-D multimode phase speed maps with a cell interval of 1.5° at

periods between 39 and 167 s for the fundamental mode, and a cell interval of 2.0° at periods between 39 and 125 s for the higher modes. The phase speed maps were then interpolated with a grid interval of 1.0° by the B-spline function.

The third stage of the three-stage inversion method was to invert the multi-mode phase speed maps for the shear wave speed model at each grid. The multi-mode phase dispersion can be represented as a function of density, P-wave speed, and shear wave speed. We fixed the density and P-wave speed structure to the reference model and solved only for shear wave speed, because the effects of the density and P-wave speed on Rayleigh wave phase speed perturbation are not

Fig. 3. Map projections of the shear wave speed at depths of (a) 40, (b) 80, (c) 120, (d) 160, (e) 200 and (f) 240 km. The reference shear wave speed profile is represented by the solid line in (g), which is the laterally averaged structure of our 3D model. The dashed line in (g) is the SV wave speed of PREM.

Shear wave speed (km/s)

(a) 40 km (b) 80 km (c) 120 km

(d) 160 km (e) 200 km (f) 240 km

(g) Shear wave speed (km/s)

dVs(%)
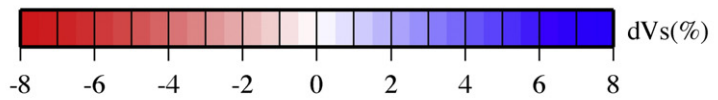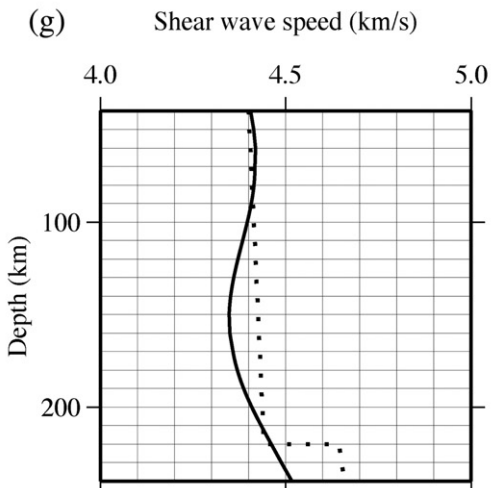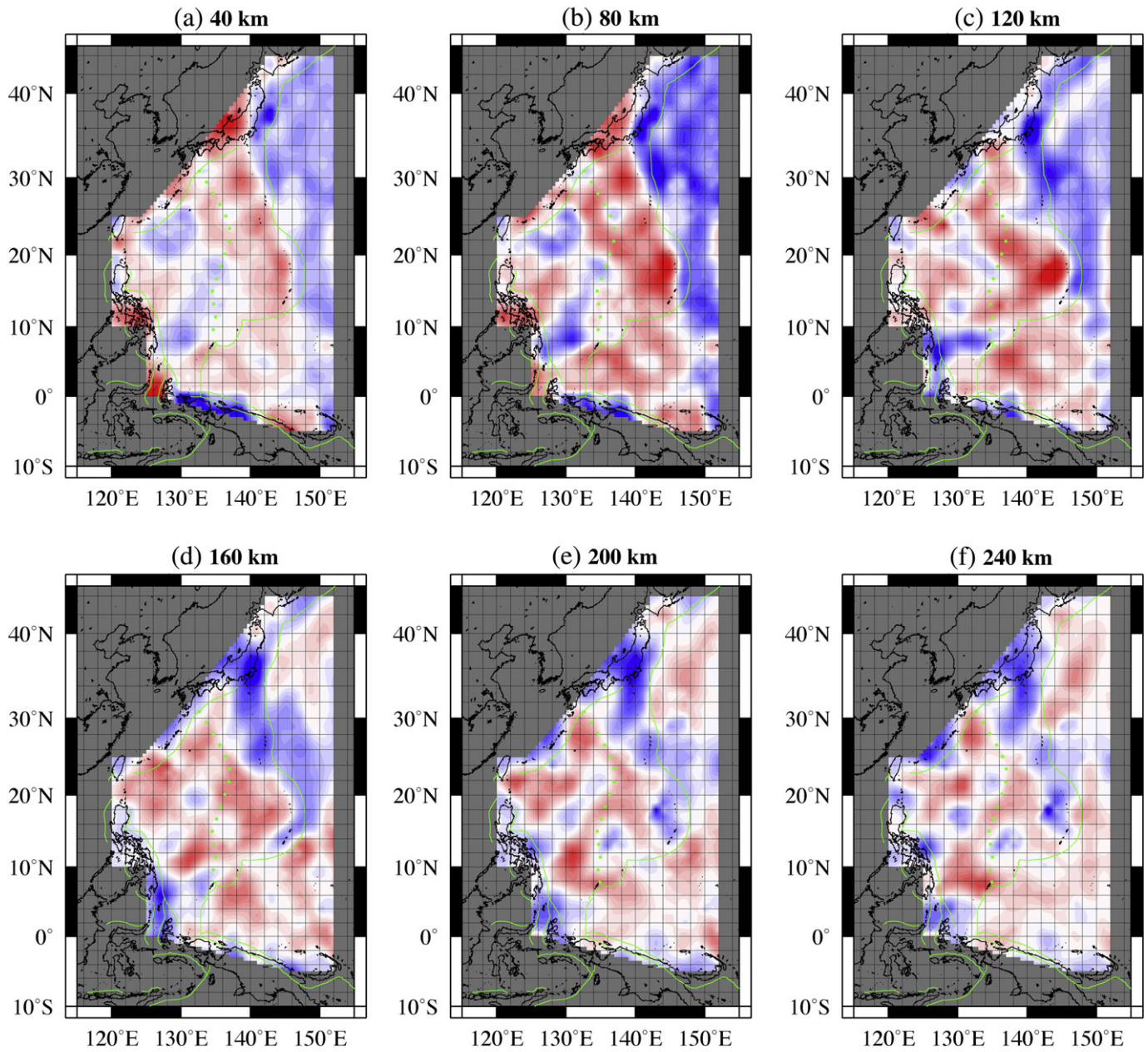
significant (Nataf et al., 1986). The iterative least squares inversion by Tarantola and Valette (1982) was used for the inversion. In this inversion, the degree of the perturbation and the smoothness of the depth variation are controlled via a priori model covariance with a Gaussian distribution. We have used a standard deviation $\sigma = 0.1$ km/s and a correlation length $L = 5$ km at a depth of up to 30 km, and $L = 20$ km at depths ranging from 30 to 670 km depth so that large perturbations are allowed in the crust. The reference 1-D model was based on PREM (Dziewonski and Anderson, 1981), except for the crust for which we adopted the CRUST2.0 model (Bassin et al., 2000).

To assess the resolution of tomographic models, we conducted two checkerboard resolution tests with cell sizes of 3 and 4° (Fig. 2) at a period of 42 s. We calculated the synthetic data from input checkerboard models using a finite frequency effect that we subsequently inverted for phase speed maps. The input checkerboard patterns are well reconstructed in the entire Philippine Sea region for a cell of 4° and in the northern Philippine Sea region for a cell of 3°. We consider the lateral resolution achieved in this study to be 3–4° within the Philippine Sea region. Lateral heterogeneities in the regions surrounding the Philippine Sea are poorly resolved.

5. Results

5.1. Shear wave speed structures in and around the Philippine Sea region

Fig. 3 shows the geographical distribution of the three-dimensional shear wave speed models obtained beneath the Philippine Sea. Recent global P-wave tomography (Li et al., 2008) showed slow speed anomalies along the IBM arc but normal values in the Philippine Sea. This is broadly consistent with our regional shear wave speed model, but further comparison is impossible because their model has less spatial resolution because it has fewer stations and events in the Philippine Sea Plate except for its rim.

At depths shallower than 80 km, the pattern of lateral variation correlates well with the age of the province. There is a sharp speed

contrast across the IBM trench, which separates the old (130–160 Ma) and cold Pacific Plate from the much younger (<50 Ma) lithosphere of the eastern Philippine Sea Plate: fast anomalies in the Pacific Ocean and slow anomalies in the eastern part of the Philippine Sea. Shear wave speeds beneath the ~150 Ma old Pacific seafloor are fastest (+3.3%), whereas those beneath the youngest seafloor age of 0–7 Ma in the Mariana Trough are slowest (−5.4%). A large-scale lateral variation in the Philippine Sea is also observed. The eastern part of the Philippine Sea plate (Shikoku and Parece Vela basins whose seafloor age is about 15–30 Ma) has slower speeds (−2.4%) than the western part (West Philippine basin whose sea floor age is about 35–50 Ma) (+0.3%). The Caroline Plate (25–40 Ma) is slow (−2.0%). To analyze the age dependence of the oceanic lithosphere in the Philippine Sea Plate and the Pacific Plate, we calculated the average shear wave speed profiles for 10 Ma intervals along isochrons of Müller et al. (2008) (Fig. 4). The Caroline Plate is not a well-solved region (Fig. 2), so we did not analyze it. Fig. 4b clearly shows the age dependence of the lithosphere.

In the western part of the Philippine Sea Plate, the old Daito Ridge province and the old plume feature of the Benham Rise are also slow. This may reflect the thick remnant arc crust and some remnant effect of a mantle plume, respectively. The fast anomalies in the southwest part may be caused by old thick lithosphere. There is a slow anomaly near the rim of the Pacific plate at about 25°N where the Ogasawara Plateau is located. The Ogasawara Plateau and a seamount chain to the east of it are a western extension of the Marcus–Wake seamount chain with relief of about 2000–3000 m relative to the adjacent ocean basin and they consist of Cretaceous guyots (Okamura et al., 1992). The crust is about 3 km thicker than beneath the adjacent ocean basin to the south of the Ogasawara plateau (Tsujii et al., 2007). This thick crust and perhaps depleted upper mantle root, as is observed beneath the Ontong–Java Plateau (Gladczenko et al., 1997), could be the cause of the slow speed anomaly.

At depths greater than 120 km, the age-dependent differences between the Pacific Plate and the Philippine Sea Plate gradually diminish (Fig. 3c–f). The most prominent fast anomalies are beneath
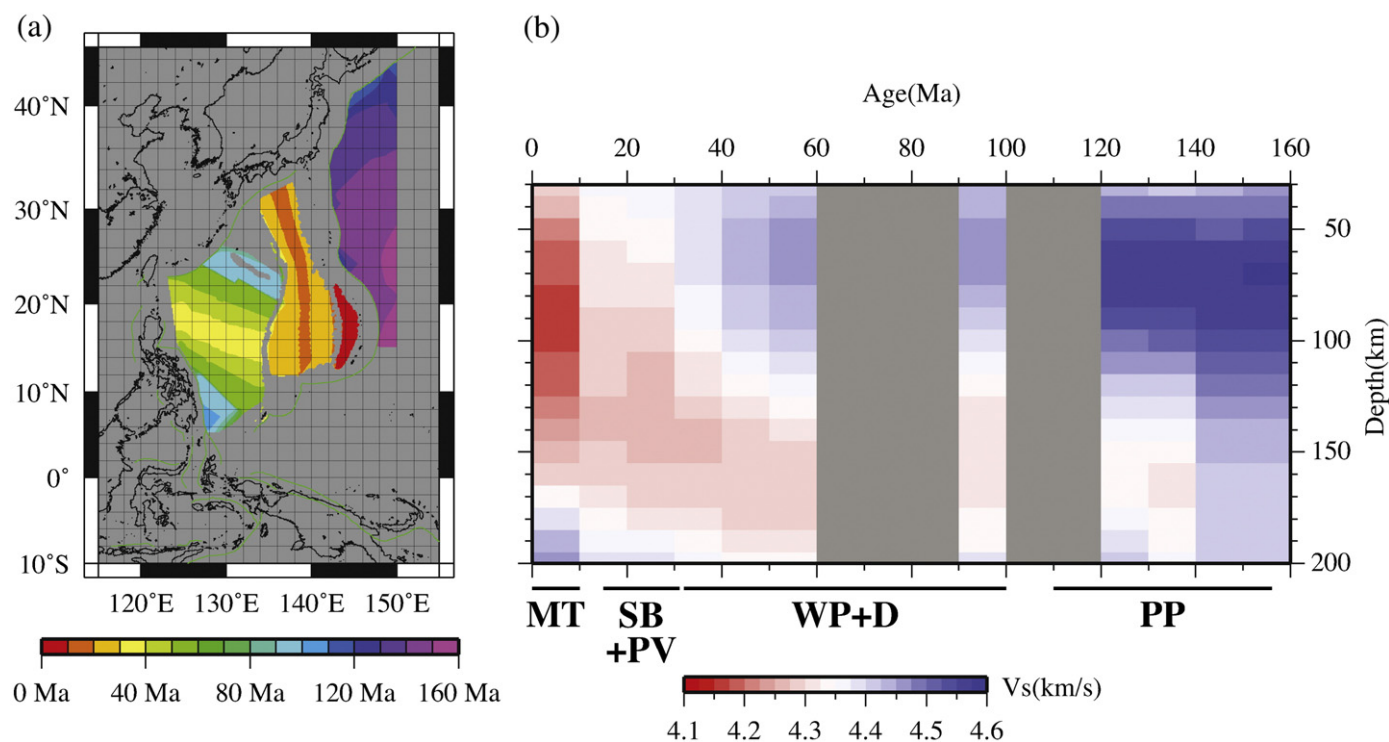

Fig. 4. (a) Distribution of ocean ages for the Philippine Sea Plate and the Pacific Plate from Müller et al. (2008) used to calculate the average shear wave depth profiles. (b) The shear wave depth profiles against the sea floor age shown in (a). Black solid lines shown below the profiles indicate the periods of seafloor ages of basins in the Philippine Sea Plate and the Pacific Plate. MT, SB+PV, WP+D, and PP indicate Mariana Trough, Shikoku Basin and Parece Vela Basin, West Philippine Basin, and Pacific Plate, respectively.
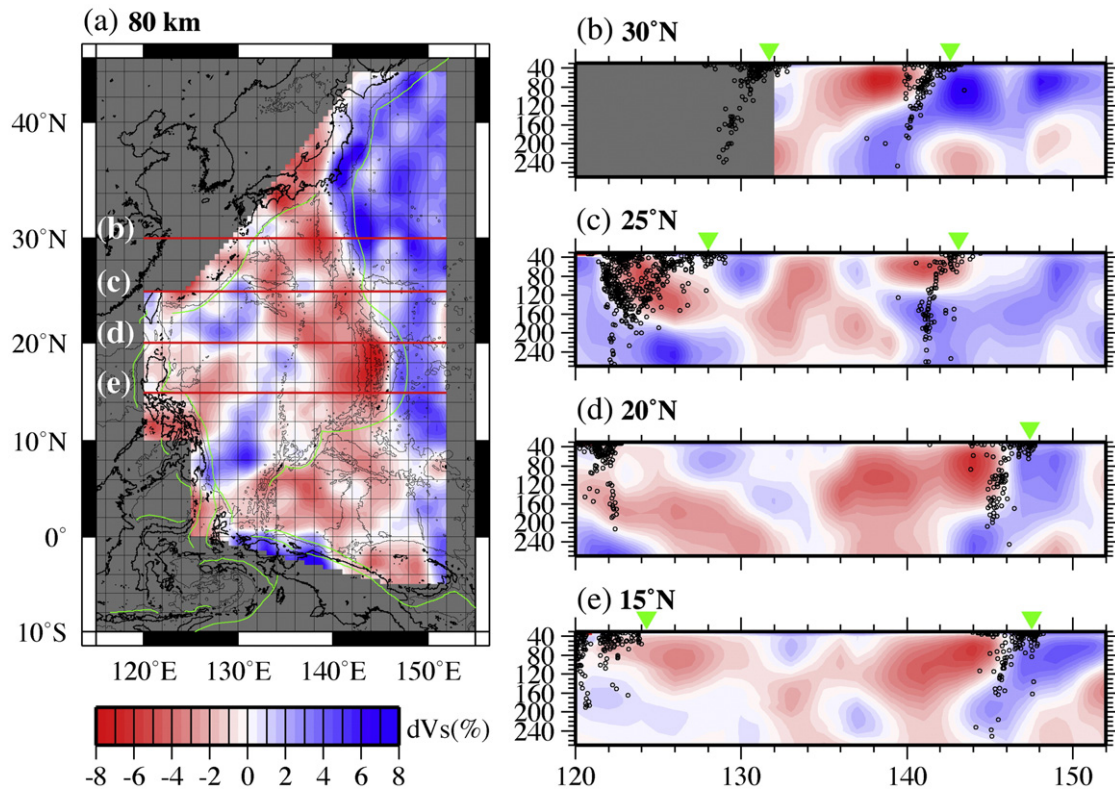
Fig. 5. (a) Map projection of the shear wave speed at depths of 80 km with the contour indicating bathymetry at a depth of 3500 m. Shear wave speed of vertical profiles along (b) 30, (c) 25, (d) 20, (e) 15°N. Green inverted triangles show the location of trenches, and black circles denote earthquake hypocenters in a 50-km-wide volume centered on each cross-section.

the IBM arc and shift westward with depth, delineating the subducted Pacific slab dipping to the west. The slow anomalies beneath the Mariana Trough, where active spreading is taking place, are present down to 160 km. Slow anomalies beneath the West Philippine Basin (WPB) are mostly parallel to the Kyushu–Palau Ridge (KPR) at depths greater than 160 km, and have not been imaged in the previous
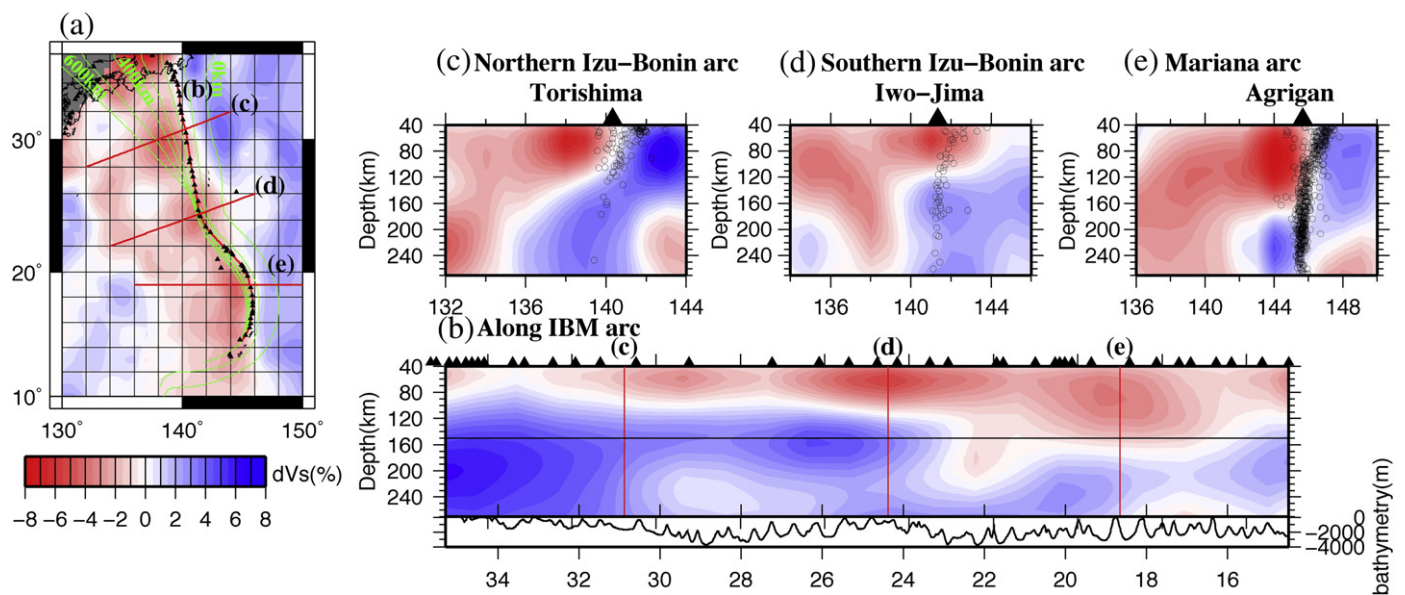

Fig. 6. Along- and across-arc depth profiles of the shear wave speed. (a) Map projection at a depth of 40 km. Lines (b–e) indicate the location of the cross-sections. The 100-km contours of the Wadati–Benioff zone are indicated as green lines. Solid triangles denote Quaternary volcanoes. (b) Vertical cross-section of shear wave speed perturbations (in percent) along the volcanic front. Along-arc profile shows three peaks of slow anomalies <120 km in depth. Solid black line shows the approximate location of the slab upper surface. lower panel shows the bathymetry along the IBM arc. Cross-sections of fractional shear wave speed perturbation (in percent) along lines (c) in the northern Izu–Bonin arc, (d) in the southern Izu–Bonin arc, and (e) in the Mariana arc. Circles denote earthquake hypocenters in a 50-km-wide volume centered on each cross-section. Locations of volcanic islands shown in (c–e) are shown in Fig. 1a.

studies. In Fig. 3e and f, specifically, fast anomalies exist west of the KPR (in the WPB) and east of the KPR (north of Yap island) whereas slow anomalies exist along the KPR and west of the WPB. Overall, the mantle beneath the Philippine Sea Plate does not have slow seismic speed.

Fig. 5 shows a longitudinal vertical profile of shear wave speed. The fast anomalies of subducting Pacific slab can be seen clearly.

5.2. Slow anomalies in the mantle wedge of the Izu–Bonin–Mariana arc

Fig. 6 shows cross-sections of shear wave speed anomaly structures in the upper mantle beneath the IBM arc. Importantly, slow speed anomalies of −6 to −11% exist within the mantle wedge of the IBM subduction zone, and are not distributed continuously along the arc. Instead, they consist of three separate anomalies centered at (30°N, 138°E), (24°N, 141°E), and (18°N, 143°E) (Figs. 3 and 6). Our previous study (Isse et al., 2006) could not resolve these anomalies because of insufficient spatial resolution.

The northern and southern anomalies clearly lie beneath the rear arc region behind the active volcanoes and rifts (Fig. 5a). The southern anomaly lies beneath the widest portion of the active-spreading Mariana Trough. The northern anomaly lies beneath the inactive rear arc seamount chains of the Izu arc west of Torishima volcano. The rift grabens behind the Izu arc lie just east of the northern anomaly. The northern and southern anomalies are of similar magnitude at 40 to 80 km depth. Consequently, whatever process is responsible for these slow speed anomalies can occur with or without spreading and regardless of the slab dip. The anomaly extends deeper where subduction is vertical in the south (beneath Agrigan). In contrast, the central anomaly (beneath Iwo Jima) is not as pronounced and seems to lie closer to the arc front.

6. Discussion

6.1. Are seismic anomalies along the IBM arc separated and located in the mantle wedge?

We found short-wavelength anomalies that have not been identified before: the three separate slow anomalies in the mantle wedge along the IBM arc.

To assess the resolution of our tomographic models along the IBM arc, we conducted a synthetic tests with two anomaly patterns: a single versus three separate sheet-shaped slow anomaly regions (Fig. 7) with 300 km width along the IBM arc at a period of 42 s. We calculated the synthetic data from input models considering the finite frequency effect and ray bending, which was subsequently inverted for phase speed maps. The input patterns are well reconstructed in both cases. The results indicate that we can distinguish three sheets from one sheet of slow anomaly. We conclude that the short wavelength anomalies along the IBM arc are separate and can be resolved by the large number of events and stations, including ocean bottom stations, and the smaller grid size used in this study. The newly found anomalies are located in well-resolved areas (Figs. 3 and 7) and cannot be explained as artifacts because of improperly modeled lateral heterogeneities.

Could the apparent separation be caused by something else? Recent crustal studies have revealed that the crustal thickness varies substantially along the IBM arc (Kodaira et al., 2007a,b). However, the pattern of crustal variation is different from that of the slow anomalies in the mantle wedge imaged by this study. The crustal variation has wavelengths of 80 and 1000 km (Kodaira et al., 2007a,b), which correspond to the spacing of basaltic volcanoes and the differences between the relatively thick Izu arc crust and the extremely thin Bonin arc crust, respectively. The slow anomalies imaged by our tomography have a wavelength of 500 km and have nothing to do with volcano spacing or crustal thickness. We also examined the relationship
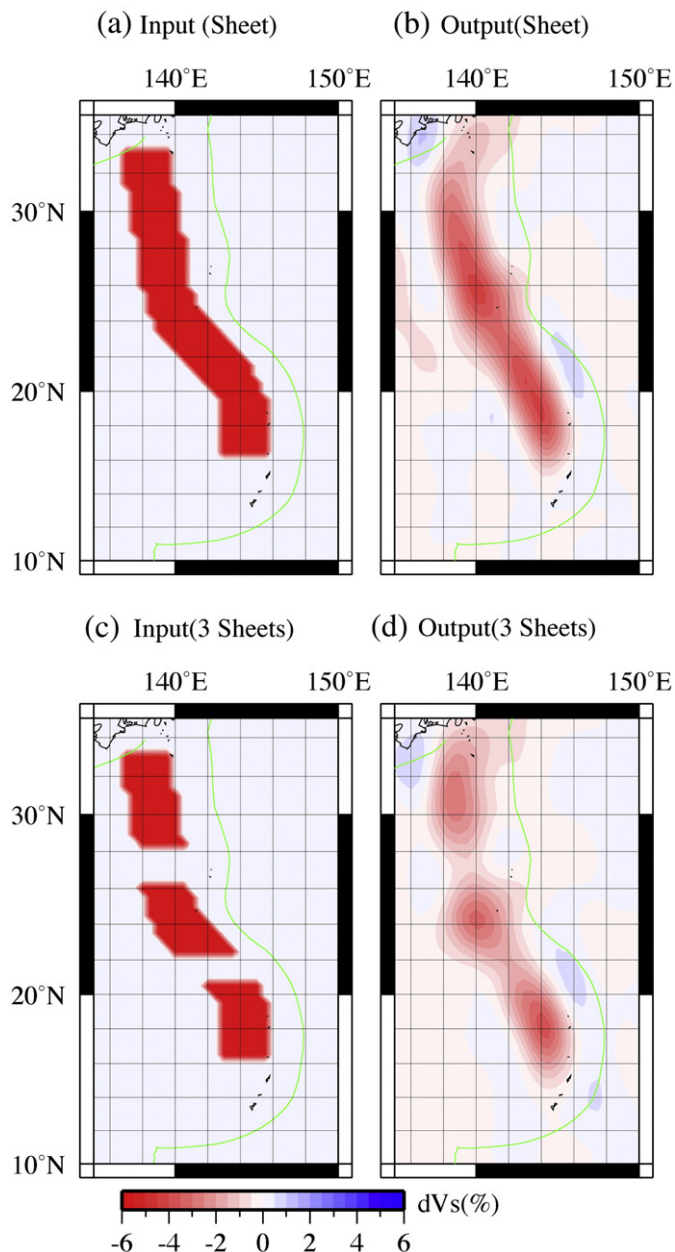

Fig. 7. Synthetic test result for the fundamental mode of 42 s: (a, b) one sheet-shaped slow anomaly with 300 km width and (c, d) three sheet-shaped anomalies. The amplitude of the anomalies is −6%. From the left to right, input models (a, c), and the output models recovered from all of the synthetic data (b, d).

between the bathymetry and shear wave speed anomalies (Fig. 6b). It seems that Iwo–Jima area at 24–25°N in the southern Izu–Bonin arc is deeper and has slower anomalies than the regions adjacent it (27.5°N and 21°N). However, the greater water depth at 24–25°N would reduce the phase speed of surface waves, which is inconsistent with our observations. This suggests that differences in water depth cannot explain the slow speed anomalies either.

The northern and southern anomalies in the mantle wedge of the IBM arc have been found by other studies using body waves but their lateral extent was not determined. Obana et al. (2007) analyzed the P- and S-wave speed structures beneath the northern Izu–Bonin arc (30–34°N in latitude) using the arrival times of local earthquakes recorded by island and ocean bottom seismographs and found slow anomalies in the mantle wedge, which corresponds to the northernmost slow anomaly obtained in this study. Shito et al. (2007) analyzed P-wave attenuation and travel time anomalies of P- and S-wave speeds in the

mantle surrounding the Izu–Bonin subduction zone (25–30°N in latitude). They found large positive travel time anomalies without comparable high attenuation in the mantle wedge, which also corresponds to the northernmost slow anomaly of the three anomalies obtained by this study (Fig. 6). The southernmost slow anomaly is located beneath the Mariana Trough, and is the deepest-rooted (120–160 km) among the three slow anomalies. Wiens et al. (2006) used a regional waveform inversion method to demonstrate low shear wave speeds beneath the Mariana Trough at ~200 km depth. Our model is consistent with their one-dimensional shear wave speed model.

6.2. What is the cause of slow anomalies along the IBM mantle wedge?

The magnitude of the slow speed anomalies found in this study (6–11%) is difficult to explain only as a thermal effect alone. The 6% anomaly in the southern Izu–Bonin segment at a depth of 60 km would require the mantle to hotter by 730 K than normal if temperature alone caused the slow anomaly, using the temperature derivative of Sobolev et al. (1996). This suggests a temperature of about 1400 K, which is hotter than the dry solidus of peridotite at 2 GPa, requiring the presence of melt. The slow shear wave speed of

6% would require up to 6 vol.% melt if it results from partial melt alone, using the theory developed by Takei (2002). Consequently, a small-amount of partial melt (less than 6 vol.%) is present in addition to high temperature. Shito et al. (2007) also proposed the presence of partial melt in the Izu–Bonin mantle wedge.

In the Mariana segment, the slow speed anomalies are located beneath the Mariana Trough, which is the only actively spreading center in this study. The average shear wave speed profile of our model (Fig. 4b) is consistent with the model of Wiens et al. (2006). The anomalies in that segment may be caused by the active melting taking place beneath the Mariana Trough.

6.3. Isotopic variation of arc front volcanoes, rear arc and rift volcanoes and Mariana Trough along the IBM subduction zone

In order to examine whether the three slow anomalies are compositionally similar to each other, we compiled $^{87}Sr/^{86}Sr$, $^{143}Nd/^{144}Nd$, and $^{206}Pb/^{204}Pb$ data for volcanic rocks in the IBM arc front volcanoes ranging from Oshima (34.72°N) to Chaife (14.66°N), and for the rear arc volcanoes and rifts of the Izu arc and the Mariana Trough (Volpe et al., 1987; Woodhead, 1989; Volpe et al., 1990; Hochstaedter et al., 1990; Lin et al., 1990; Stern et al., 1993; Gribble et al., 1996; Elliott
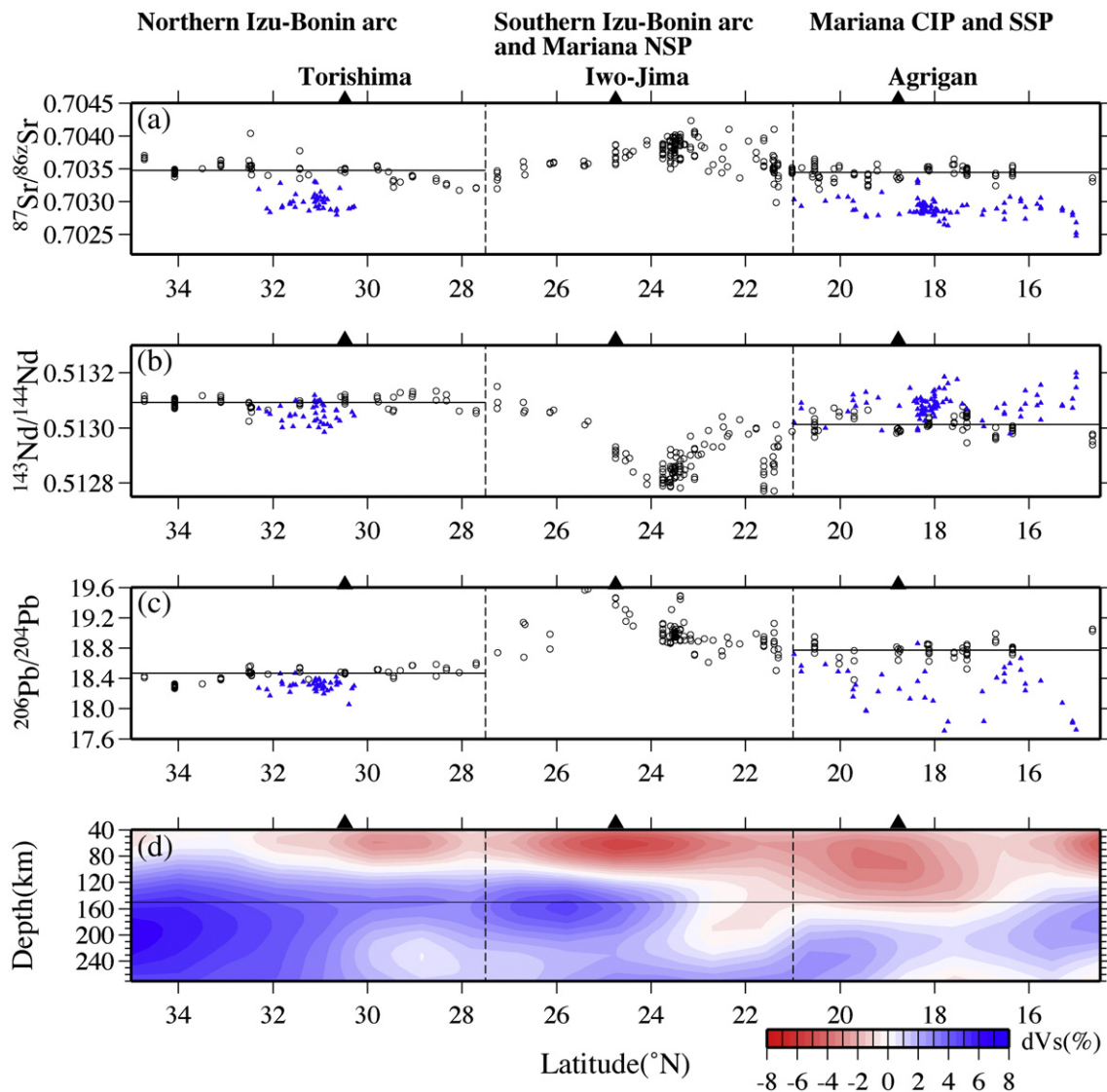
Fig. 8. Along-arc variation of (a) $^{87}Sr/^{86}Sr$, (b) $^{143}Nd/^{144}Nd$ and (c) $^{206}Pb/^{204}Pb$ values of frontal arc volcanoes (circles) and rear arc volcanoes of northern Izu and the Mariana Trough (blue triangles). (d) Along-arc shear wave speed profiles the same as in Fig. 5b. Solid black line indicates the approximate location of the slab upper surface. The locations of volcanic islands shown in (a–d) are shown in Fig. 1a.

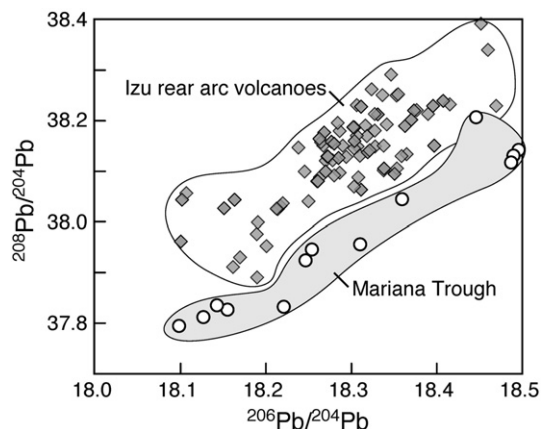**Fig. 9.** $^{208}Pb/^{204}Pb$ vs $^{206}Pb/^{204}Pb$ of the Izu rear arc and Mariana rear arc (Mariana trough) lavas. Izu rear arc lavas are systematically higher in $^{208}Pb/^{204}Pb$ at the same $^{206}Pb/^{204}Pb$ than Mariana rear arc, suggesting different mantle domains between Izu and Mariana.

et al., 1997; Gribble et al., 1998; Taylor and Nesbitt, 1998; Hochstaedter et al., 2001; Sun and Stern, 2001; Kuritani et al., 2003; Stern et al., 2003; Yokoyama et al., 2003; Tamura et al., 2005; Wade et al., 2005; Kohut et al., 2006; Stern et al., 2006; Yokoyama et al., 2006; Ishizuka et al., 2007; Ishizuka unpublished data). Fig. 8 shows the along-arc variation of isotope ratios.

$^{87}Sr/^{86}Sr$ decreases gradually from north to south in the Izu–Bonin arc between 35°N and 27.5°N. However, south of 27.5°N, the isotopic trend is reversed with $^{87}Sr/^{86}Sr$ increasing southward (Taylor and Nesbitt, 1998; Ishizuka et al., 2007). The maximum $^{87}Sr/^{86}Sr$ appear in arc volcanoes between 21°N and 25°N in the shoshonitic province in the southern Izu–Bonin arc and NSP of the Mariana arc (Sun and Stern, 2001). Volcanoes in the CIP and SSP of the Mariana arc have lower and more constant $^{87}Sr/^{86}Sr$ values, which are similar to those from the northern Izu–Bonin arc (Fig. 8a).

$^{143}Nd/^{144}Nd$ variations along the arc are the inverse of Sr isotopes, with the shoshonitic province of the southern Izu–Bonin arc and NSP of the Mariana arc volcanoes having less radiogenic Nd than the rest of the arc (Stern et al., 2003). $^{143}Nd/^{144}Nd$ values of the Mariana arc (CIP and SSP) are lower than those of the northern Izu–Bonin arc (Fig. 8b).

$^{206}Pb/^{204}Pb$ increases continuously toward the south in the Izu–Bonin arc, but increases sharply south of 27.7°N to reach a maximum of ~19.6 at Kitaiwo–jima island (Taylor and Nesbitt, 1998; Ishizuka et al., 2007). Ishizuka et al. (2007) showed that trace element ratios also show systematic along-arc variation from north (35°N) to south (24.5°N). $^{206}Pb/^{204}Pb$ values of the Mariana arc (CIP and SSP) are higher than those of the northern Izu–Bonin arc (Fig. 8c).

The IBM volcanic front can be divided into three geographic segments based on the isotope ratios and the degree of isotopic variability. The Izu–Bonin segment north of 27.5°N is characterized by high $^{143}Nd/^{144}Nd$ (0.513093 on average) and low $^{206}Pb/^{204}Pb$ (18.47 on

average). The volcanoes in the southern Izu–Bonin arc and the NSP of the Mariana arc between 27.5°N and 21°N (shoshonitic province) have the highest $^{87}Sr/^{86}Sr$ and $^{206}Pb/^{204}Pb$, and the lowest $^{143}Nd/^{144}Nd$. Isotopic variability within this segment is characteristically large. The Mariana CIP and SSP segments, south to 21°N, are distinguished by lower $^{87}Sr/^{86}Sr$ (0.703443 on average) and $^{143}Nd/^{144}Nd$ (0.513013 on average), and higher $^{206}Pb/^{204}Pb$ (18.7741 on average) compared with that in the northern Izu–Bonin arc.

In contrast, the rear arc volcanoes of the Izu and Mariana arcs cannot be distinguished from one another using the isotope ratios in Fig. 8. However, there are consistent differences in their Pb isotope ratios. The Izu rear arc has a more Indian Ocean-type isotopic signature whereas the Mariana Trough has a more Pacific-type signature (Hickey-Vargas, 1998). The isotopic signatures of rear arc volcanoes are less affected by fluid-mobile recycled slab components so that the difference between them better reflects the mantle being imaged in the northern and southern anomalies independent of current subduction.

The along-strike differences in isotope ratios at both the volcanic front and rear arc correlate with the along-strike differences in shear wave speed anomalies. Those shown in Fig. 8 for the volcanic front probably are inherited from the currently subducting slab (Plank et al., 2007, and all references above about isotopes). Ishizuka et al. (2007) suggested that the volcaniclastic sediments originating from HIMU oceanic islands on the subducting Pacific plate are possible candidates to introduce a component with high $^{206}Pb/^{204}Pb$ and low $^{143}Nd/^{144}Nd$ into mantle wedge between 25°N and 27.5°N. In contrast, the differences shown in Fig. 9 apply to the rear arc which is less affected by slab components and coincides more closely with the location of the shear wave anomalies. Consequently the rear arc differences may reflect the mantle independent of current subduction.

6.4. Do the slow anomalies in the mantle wedge along the IBM arc represent mantle return flow?

Subduction of the Pacific Plate beneath the Philippine Sea Plate causes convection within the intervening mantle wedge. However, how and where does the deeper part of the upper mantle enter the wedge? Is it continuous along the 2800-km IBM arc? We suggest that upper mantle enters the wedge of the IBM subduction zone at the three slow anomalies spaced 500 km apart. Because the isotope ratios are insensitive to temperature differences or extents of partial melting, they suggest that mantle entering the wedge and flowing from the rear arc to the volcanic front is not chemically uniform along the IBM arc.

The correlation between isotope systematics and seismic speed is one of the new and unexpected findings of this study. We suggest that mantle convection produces three different upwelling zones along the IBM arc each with slightly different mantle (Fig. 10). The isotopic difference between lavas in the Izu versus Mariana rear arcs indicates that the mantle is heterogeneous along-strike independent of current subduction. Slab components also differ along strike and can explain
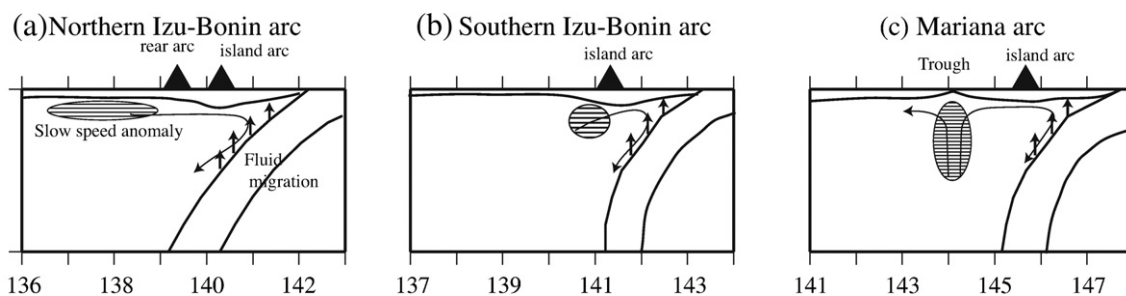

Fig. 10. Cartoon of the mantle wedge beneath (a) the northern Izu–Bonin arc, (b) southern Izu–Bonin arc, and (c) Mariana arc, respectively. The mantle flow to the island arc should be horizontal in the northern Izu–Bonin arc, whereas it should be vertical in the Mariana arc.

the isotopic differences along the volcanic front. Each of the three upwelling zones is isotopically distinct and the sum of these two processes.

Shear wave splitting measurements also provide significant information about flow directions in the mantle wedge. There are only a few result so far the IBM arc. Fouch and Fischer (1998) found fast orientations roughly parallel to the absolute plate motion (APM) of the Pacific Plate near Guam. Volti et al. (2006) also found similar results in the Mariana volcanic front using OBS data, but they found fast orientations sub-parallel to the spreading direction in the Mariana Trough. Pozgay et al. (2007) found complex fast orientations in the Mariana arc using data recorded by dense temporary land and seafloor seismological arrays. Between 17.5° and 19°N, fast orientations are parallel to the arc beneath the arc and between it and the back-arc spreading center for events <250 km depth; fast orientations are somewhat different for deeper events. Between 15° and 17.5°N, fast orientations beneath the arc are sub-parallel to the arc and the APM for events <250 km depth and parallel to the APM for deeper events. In the Marianas, fast orientations range from arc-perpendicular to APM-parallel west of the Mariana Trough spreading center, but they are arc-parallel in the arc with variable orientations surrounding Guam. Pozgay et al. (2007) concluded that arc-parallel mantle flow is the cause of the arc-parallel fast orientations and that the typical interpretation of mantle wedge flow strongly coupled to the down-going slab is only valid at depths greater than 250 km and at large distances from the trench. Anglin and Fouch (2005) analyzed the shear wave splitting beneath the Izu–Bonin arc between 26°N and 34°N and found that the fast orientation directions were approximately NNW–SSE between 26°N and 29.5°N (oblique to the trench) and were approximately NNE–SSW (nearly parallel to the trench) between 29.5°N and 34°N. Our northernmost slow anomalies are located in their northern region while the gap between northernmost and central slow anomalies is located in their southern region.

These results indicate that azimuthal variations of shear wave splitting are very complicated in the IBM arc and that mantle flow along the arc is not uniform, which is consistent with our suggestion.

Tamura et al. (2002) showed that Quaternary volcanoes in the NE Japan arc can be grouped into 10 elongate volcanic groups striking transverse to the arc. They concluded that mantle melting and the production of magmas in NE Japan may be controlled by locally developed hot regions within the mantle wedge that have the form of inclined, 50-km-wide fingers, which can be clearly seen as an inclined slow-speed zones in the high-resolution body wave tomography of Hasegawa and Nakajima (2004). However, their model has poor resolution in the rear arc region beneath the Japan Sea due to not having seismic stations there, so the root of the hot fingers is unconstrained in that region.

The spacing of basaltic volcanoes is 50–100 km in the IBM arc (Kodaira et al., 2007a,b), and if hot fingers exist beneath these volcanoes, the wavelength of anomalies should be less than 100 km as in NE Japan arc. However, this study has a spatial resolution of ~300 km which is not high enough to detect the hot fingers.

We speculate here that deep mantle enters the wedge of the IBM subduction zone at the three slow anomalies spaced 500 km apart, and then branches into hot fingers as it ascends toward the volcanic front. This can explain the complex shear wave splitting in the Izu–Bonin arc. We do not know what controls the 500 km spacing, but each "arc" segment seems to have a separate mantle feeder with different Pb isotopes (Fig. 9). All the isotopic differences, as shown in Fig. 8, may be inherited from the slab, and added to the mantle deep enough in the system to characterize the "palm" before it branches into "fingers," or they may be added only to the finger-tips beneath the volcanic front. In contrast, the underlying more "Pacific" character of the Pb in the southern anomaly is consistent with mantle flow around the southern edge of the Pacific Plate. A similar along-strike variation in the mantle exists in the northern Lau Basin and Tonga arc (Pearce

et al., 2007). Higher resolution tomography of short-period body waves using more OBS will be required to test this hypothesis.

7. Conclusions

We have determined the three-dimensional shear wave speed structure in and around the Philippine Sea and applied an inversion technique of surface wave tomography, incorporating the effects of finite frequency and ray bending. The new BBOBS data, along with the increased number of events used, enable us to obtain better spatial resolution than in previous studies. Our model reveals three slow anomalies of shear wave speed structures at the scale of 500 km in the mantle wedge along the IBM arc. This variation is well correlated with the along-arc variations of isotopes, suggesting that the mantle flow in the mantle wedge along the IBM arc is not a continuous sheet-like flow but is separated into three isotopically distinct segments.

Acknowledgements

Appendix A. Supplementary data

Supplementary data associated with this article can be found, in the online version, at doi:10.1016/j.epsl.2008.11.032.

References

Anglin, D.K., Fouch, M.J., 2005. Seismic anisotropy in the Izu–Bonin subduction system. Geophys. Res. Lett. 32, L09307. doi:10.1029/2005GL022714.

Bassin, C., Laske, G., Masters, G., 2000. The current limits of resolution for surface wave tomography in North America. Eos Trans AGU Fall Meet. Suppl., 81, Abstract, S12A-03.

Bloomer, S.H., Stern, R.J., Smoot, N.C., 1989. Physical volcanology of the submarine Mariana and Volcano arcs. Bull. Volcanol. 51, 210–224.

Bloomer, S.H., Taylor, B., MacLeod, C.J., Stern, R.J., Fryer, P., Hawkins, J.W., Johnson, L., 1995. Early arc volcanism and the Ohiolite problem: a perspective from drilling in the western Pacific. In: Taylor, B., Natland, J. (Eds.), Active Margins and Marginal Basins of the Western Pacific. Geophysical Monograph, vol. 88. AGU, Washington, D.C., pp. 1–30.

Deschamps, A., Lallemand, S., 2002. The west Philippine basin: an Eocene to early Oligocene back arc basin opened between two opposed subduction zones. J. Geophys. Res. 107, 2322. doi:10.1029/2001JB001706.

Dziewonski, A.M., Anderson, D.L., 1981. Preliminary reference Earth model. Phys. Earth Planet. Inter. 25, 297–356.

Elliott, T., Plank, T., Zindler, A., White, W., Bourdon, B., 1997. Element transport from slab to volcanic front at the Mariana arc. J. Geophys. Res. 102, 14,991–15,019.

Fouch, M.J., Fischer, K.M., 1998. Shear wave anisotropy in the Mariana subduction zone. Geophys. Res. Lett. 25, 1221–1224.

Fukao, Y., Morita, Y., Shinohara, M., Kanazawa, T., Utada, H., Toh, H., Kato, T., Sato, T., Shiobara, H., Seama, N., Fujimoto, H., Takeuchi, N., 2001. The Ocean Hemisphere Network Project (OHP). Workshop Report of OHP/ION Joint Symposium, Long-Term Observations in the Oceans. Earthquake Res. Inst., Univ. of Tokyo, Tokyo, pp. 13–29.

Fukuyama, E., Ishida, M., Hori, S., Sekiguchi, S., Watada, S., 1996. Broadband seismic observation conducted under the FREESIA Project. Rep. Natl. Res. Inst. Earth Sci. Disaster Prevent. 57, 23–31.

Gill, J.B., Hiscott, R.N., Vidal, Ph., 1994. Turbidite geochemistry and evolution of the Izu–Bonin arc and continents. Lithos 33, 135–168.

Gladczenko, T.P., Coffin, M.F., Eldholm, O., 1997. Crustal structure of the Ontong Java Plateau: modeling of new gravity and existing seismic data. J. Geophys. Res. 102, 22,711–22,729.

Goldstein, P., Minner, L., 1996. SAC2000: seismic signal processing and analysis tools for the 21st century. Seismol. Res. Lett. 67, 39.

Gorbatov, A., Kennett, B.L.N., 2003. Joint bulk-sound and shear tomography for Western Pacific subduction zones. Earth Planet. Sci. Lett. 210, 527–543.

Gribble, R.F., Stern, R.J., Bloomer, S.H., Stuben, D., O'Hearn, T., Newman, S., 1996. MORB mantle and subduction components interact to generate basalts in the southern Mariana Trough back-arc basin. Geochim. Cosmochim. Acta 60, 2153–2166.

Gribble, R.F., Stern, R.J., Newman, S., Bloomer, S.H., O'Hearn, T., 1998. Chemical and isotopic composition of lavas from the Northern Mariana Trough: implications for magmagenesis in back-arc basins. J. Petrol. 39, 125–154.

Hall, R., 2002. Cenozoic geological and plate tectonic evolution of SE Asia and the SW Pacific: computer-based reconstructions, model and animations. J. Asian Earth Sci. 20, 353–431.

Hall, C.E., Gurnis, M., Sdrolias, M., Lavier, L.L., Müller, R.D., 2003. Catastrophic initiation of subduction following forced convergence across fracture zones. Earth Planet. Sci. Lett. 212, 15–30.

Hasegawa, A., Nakajima, J., 2004. Geophysical constraints on slab subduction and arc magmatism. In: Sparks, R.S.J., Hawkesworth, C.J. (Eds.), The State of the Planet: Frontiers and Challenges in Geophysics. Geophysical Monograph, vol. 150. AGU, Washington D. C., pp. 81–94.

Hickey-Vargas, R., 1998. Origin of the Indian Ocean-type isotopic signature in basalts from Philippine Sea plate spreading centers; an assessment of local versus large-scale processes. J. Geophys. Res. 103, 20,963–20,979.

Hickey-Vargas, R., Savov, I.P., Bizimis, M., Ishii, T., Fujioka, K., 2006. Origin of diverse geochemical signatures in igneous rocks from the West Philippine Basin: implications for tectonic models. In: Christie, D.M., Fisher, C., Lee, S.-M., Givens, S. (Eds.), Back-Arc Spreading Systems: Geological, Biological, Chemical and Physical Interactions. Geophysical Monograph, vol. 166. AGU, Washington D. C., pp. 287–303.

Hochstaedter, A.G., Gill, J.B., Morris, J.D., 1990. Volcanism in the Sumisu Rift, II. Subduction and non-subduction related components. Earth Planet. Sci. Lett. 100, 195–209.

Hochstaedter, A., Gill, J., Peters, R., Broughton, P., Holden, P., 2001. Across-arc geochemical trends in the Izu–Bonin arc: contributions from the subducting slab. Geochem. Geophys. Geosyst. 2 (2000GC000105).

Hussong, D.M., Uyeda, S., 1981. Tectonic processes and the history of the Mariana arc: a synthesis of the results of deep sea drilling project leg 60. Initial Rep. Deep Sea Drill. Proj. 60, 909–929.

Ishizuka, O., Kimura, J., Li, Y.B., Stern, R.J., Reagan, M.K., Taylor, R.N., Ohara, Y., Bloomer, S.H., Ishii, T., Hargrove III, U.S., Haraguchi, S., 2006. Early stages in the evolution of Izu–Bonin arc volcanism: new age, chemical, and isotopic constraints. Earth Planet. Sci. Lett. 250, 385–401.

Ishizuka, O., Taylor, R.N., Yuasa, M., Milton, J.A., Nesbitt, R.W., Uto, K., Sakamoto, I., 2007. Processes controlling along-arc isotopic variation of the southern Izu–Bonin arc. Geochem. Geophys. Geosyst. 8, Q06008. doi:10.1029/2006GC001475.

Isse, T., Shiobara, H., Fukao, Y., Mochizuki, K., Kanazawa, T., Sugioka, H., Kodaira, S., Hino, R., Suetsugu, D., 2004. Rayleigh wave phase velocity measurements across the Philippine Sea from a broad-band OBS array. Geophys. J. Int. 158, 257–266.

Isse, T., Yoshizawa, K., Shiobara, H., Shinohara, M., Nakahigashi, K., Mochizuki, K., Sugioka, H., Suetsugu, D., Oki, S., Kanazawa, T., Suyehiro, K., Fukao, Y., 2006. Three-dimensional shear wave structure beneath the Philippine Sea from land and ocean bottom broadband seismograms. J. Geophys. Res. 111, B06310. doi:10.1029/2005JB003750.

Kanamori, H., Abe, K., 1968. Deep structure of island arcs as revealed by surface waves. Bull. Earthq. Res. Inst. Univ. Tokyo 46, 1001–1025.

Kanazawa, T., Shiobara, H., Mochizuki, M., Shinohara, M., Araki, E., 2001. Seismic observation system on the sea floor. Proceedings of OHP/ION Joint Symposium, Long-Term Observations in the Oceans. Earthq. Res. Inst., Univ. of Tokyo, Tokyo, pp. S11–06.

Kennett, B.L.N., Yoshizawa, K., 2002. A reappraisal of regional surface wave tomography. Geophys. J. Int. 150, 37–44.

Kodaira, S., Sato, T., Takahashi, N., Ito, A., Tamura, Y., Tatsumi, Y., Kanada, Y., 2007a. Seismological evidence for variable growth of crust along the Izu intraoceanic arc. J. Geophys. Res. 122. doi:10.1029/2006JB004593.

Kodaira, S., Sato, T., Takahashi, N., Miura, S., Tamura, Y., Tatsumi, Y., Kaneda, Y., 2007b. New seismological constraints on growth of continental crust in the Izu–Bonin intra-oceanic arc. Geology 35, 1031–1034.

Kohut, E.J., Stern, R.J., Kent, A.J.R., Nielsen, R.L., Bloomer, S.H., Leybourne, M., 2006. Evidence for adiabatic decompression melting in the southern Mariana arc from high-Mg lavas and melt inclusions. Contrib. Mineral. Petrol. 152, 201–221.

Kuritani, T., Yokoyama, T., Kobayashi, K., Nakamura, E., 2003. Shift and rotation of composition trends by magma mixing: 1983 eruption at Miyake-jima volcano, Japan. J. Petrol. 44, 1895–1916.

Lebedev, S., Nolet, G., van der Hilst, R.D., 1997. The upper mantle beneath the Philippine Sea region from waveform inversions. Geophys. Res. Lett. 24, 1851–1854.

Li, C., van der Hilst, R.D., Engdahl, E.R., Burdick, S., 2008. A new global model for P wave speed variations in Earth's mantle. Geochem. Geophys. Geosyst 9, Q05018. doi:10.1029/2007GC001806.

Lin, P.N., Stern, R.J., Morris, J., Bloomer, S.H., 1990. Nd- and Sr-isotopic compositions of lavas from the northern Mariana and southern Volcano arcs; implications for the origin of island arc melts. Contrib. Mineral. Petrol. 105, 381–392.

Malyarenko, A.N., Lelikov, E.P., 1995. Granites and associated rocks in the Philippine Sea and the East China Sea. In: Tokuyama, H., Shcheka, S., Isezaki, N., Vysotskiy, S., Kulinich, R., Karp, B., Lelikov, E., Fujioka, K., Liu, G. (Eds.), Geology and Geophysics of the Philippine sea. Terrapub, Tokyo, pp. 311–328.

Müller, R.D., Sdrolias, M., Gaina, C., Roest, W.R., 2008. Age, spreading rates, and spreading asymmetry of the world's ocean crust. Geochem. Geophys. Geosyst 9, Q04006. doi:10.1029/2007GC001743.

Nakamura, Y., Shibutani, T., 1998. Three-dimensional shear wave velocity structure in the upper mantle beneath the Philippine Sea region. Earth Planets Space 939–952.

Nataf, H.C., Nakanishi, I., Anderson, D.L., 1986. Measurements of mantle wave velocities and inversion for lateral heterogeneities and anisotropy, 3. Inversion. J. Geophys. Res. 91, 7261–7307.

Obana, K., Kamiya, S., Kodaira, S., Suetsugu, D., Takahashi, N., Takahashi, T., Tamura, Y., Sakaguchi, H., 2007. OBS seismicity observations for crustal structure analysis in Northern Izu–Bonin arc. Abstracts of Japan Geoscience Union Meeting, J245-P011.

Oda, H., Senna, N., 1994. Regional variation in surface wave group velocities in the Philippine Sea. Tectonophysics 233, 265–277.

Okamura, Y., Murakami, F., Kishimoto, K., Saito, E., 1992. Seismic profiling survey of the Ogasawara Plateau and Michelson Ridge, western Pacific: evolution of Cretaceous guyots and deformation of a subducting oceanic plateau. Bull. Geol. Surv. Jpn. 43, 237–256.

Okino, K., Ohara, Y., Kasuga, S., Kato, Y., 1999. The Philippine Sea: new survey results reveal the structure and the history of the marginal basins. Geophys. Res. Lett. 26, 2287–2290.

Pearce, J.A., Kempton, P.D., Gill, J.B., 2007. Hf–Nd evidence for the origin and distribution of mantle domains in the SW Pacific. Earth Planet. Sci. Lett. 260, 98–114.

Plank, T., Kelley, K.A., Murray, R.W., Stern, L.Q., 2007. Chemical composition of sediments subducting at the Izu–Bonin trench. Geochem. Geophys. Geosyst. 8, Q04I16. doi:10.1029/2006GC001444.

Pozgay, S.H., Wiens, D.A., Conder, J.A., Shiobara, H., Sugioka, H., 2007. Complex mantle flow in the Mariana subduction system: evidence from shear wave splitting. Geophys. J. Int. 170, 371–386.

Sambridge, M., 1999. Geophysical inversion with a neighbourhood algorithm — I. Searching a parameter space. Geophys. J. Int. 138, 479–494.

Seno, T., Stern, S., Gripp, A.E., 1993. A model for the motion of the Philippine sea plate consistent with NUVEL-1 and geological data. J. Geophys. Res. 98, 17941–17948.

Shiobara, H., Kato, M., Sugioka, H., Yoneshima, S., Mochizuki, K., Mochizuki, M., Kodaira, S., Hino, R., Shinohara, M., Kanazawa, T., 2001. Long term observation by ocean bottom seismometer array on trans-PHS profile. Proceedings of OHP/ION Joint Symposium, Long-Term Observations in the Oceans. Earthquake Res. Inst., Univ. of Tokyo, Tokyo, pp. S11-10.

Shiobara, H., Goto, T., Sugioka, H., Baba, K., Kawakatsu, H., Shito, A., Ichikita, T., Adam, C., Ichiki, M., Koyama, T., Kanazawa, T., Utada, H., 2006. Research on the stagnat slab by long-term BBOBS and OBEM arrays. Eos Trans. AGU, Fall Meet. Suppl., Abstract, vol. 87. T51C-1545.

Shito, A., Shiobara, H., Sugioka, H., Ito, A., Kawakatsu, H., Adam, C., Kanazawa, T., 2007. Seismic velocity and attenuation in Izu–Bonin subduction zone inferred from BBOBS data. Eos Trans. AGU, Fall Meet. Suppl., Abstract, vol. 88. T51B-0555.

Shukuno, H., Tamura, Y., Tani, K., Chang, Q., Suzuki, T., Fiske, R.S., 2006. Origin of silicic magmas and the compositional gap at Sumisu submarine caldera, Izu–Bonin arc, Japan. J. Volcanol. Geotherm. Res. 156, 187–216.

Sobolev, S.V., Zeyen, H., Stoll, G., Werling, F., Altherr, R., Fuchs, K., 1996. Upper mantle temperatures from teleseismic tomography of French Massif Central including effects of composition, mineral reactions, anharmonicity, anelasticity and partial melt. Earth Planet. Sci. Lett. 139, 147–163.

Stern, R.J., 2004. Subduction initiation: spontaneous and induced. Earth Planet. Sci. Lett. 226, 275–292.

Stern, R.J., Jackson, M.C., Fryer, P., Ito, E., 1993. O, Sr, Nd and Pb isotopic composition of the Kasuga Cross-Chain in the Mariana Arc; a new perspective on the K–h relationship. Earth Planet. Sci. Lett. 119, 459–475.

Stern, R.J., Fouch, M.J., Klemperer, S.L., 2003. An overview of the Izu–Bonin–Mariana subduction factory. In: Eiler, J. (Ed.), Inside the Subduction Factory. Geophysical Monograph, vol. 138. AGU, Washington, DC, pp. 175–222.

Stern, R.J., Kohut, E., Bloomer, S.H., Leybourne, M., Fouch, M., Vervoort, J., 2006. Subduction factory processes beneath the Guguan cross-chain, Mariana Arc: no role for sediments, are serpentinites important? Contrib. Mineral. Petrol. 151, 202–221.

Sun, C.-H., Stern, R.J., 2001. Genesis of Mariana shoshonites: contribution of the subduction component. J. Geophys. Res. 106, 589–608.

Suyehiro, K., Takahashi, N., Ariie, Y., Yokoi, Y., Hino, R., Shinohara, M., Kanazawa, T., Hirata, N., Tokuyama, H., Taira, A., 1996. Continental crust, crustal underplating, and low-Q upper mantle beneath an oceanic island arc. Science 272, 390–392.

Takahashi, N., Kodaira, S., Klemperer, S.L., Tatsumi, Y., Kaneda, Y., Suyehiro, K., 2007. Crustal structure and evolution of the Mariana intra-oceanic island arc. Geology 35, 203–206.

Takei, Y., 2002. Effect of pore geometry on Vp/Vs: from equilibrium geometry to crack. J. Geophys. Res. 107. doi:10.1029/2001JB000522.

Takeuchi, H., Saito, M., 1972. Seismic surface waves. In: Bolt, E.A. (Ed.), Seismology: Surface Waves and Free Oscillations, Methods Comput. Pys., vol. 11. Academic, San Diego, pp. 217–295.

Tamura, Y., Tatsumi, Y., 2002. Remelting of an andesitic crust as a possible origin for rhyolitic magma in oceanic arcs: an example from the Izu–Bonin arc. J. Petrol. 43, 1029–1047.

Tamura, Y., Tatsumi, Y., Zhao, D., Kido, Y., Shukuno, H., 2002. Hot fingers in the mantle wedge: new insights into magma genesis in subduction zones. Earth Planet. Sci. Lett. 197, 105–116.

Tamura, Y., Tani, K., Ishizuka, O., Chang, Q., Shukuno, H., Fiske, R.S., 2005. Are arc basalts dry, wet, or both? Evidence from the Sumisu caldera volcano, Izu–Bonin arc, Japan. J. Petrol. 46, 1769–1803.

Tarantola, A., Valette, B., 1982. Generalized nonlinear inverse problems solved using the least squares criterion. Rev. Geophys. Space Phys. 20, 219–232.

Taylor, B., 1992. Rifting and the volcanic–tectonic evolution of the Izu–Bonin–Mariana arc. In: Taylor, B., Fujioka, K., et al. (Eds.), Proc. ODP Sci. Results, vol. 126. Ocean Drilling Program, College Station, TX, pp. 627–651.

Taylor, B., Goodliffe, A.M., 2004. The West Philippine Basin and the initiation of subduction, revisited. Geophys. Res. Lett. 31. doi:10.1029/2004GL020136.

Taylor, R.N., Nesbitt, R.W., 1998. Isotopic characteristics of subduction fluids in an intra-oceanic setting, Izu–Bonin Arc, Japan. Earth Planet. Sci. Lett. 164, 79–98.

Tsujii, T., Nakamura, Y., Tokuyama, H., Coffin, M.F., Koda, K., 2007. Oceanic crust and Moho of the Pacific plate in the eastern Ogasawara plateau region. Island Arc 16, 361–373.

Volpe, A.M., Macdougall, J.D., Hawkins, J.W., 1987. Mariana Trough Basalts (MTB): trace element and Sr–Nd isotopic evidence for mixing between MORB-like and arc-like melts. Earth Planet. Sci. Lett. 82, 241–254.

Volpe, A.M., Macdougall, J.D., Lugmair, G.W., Hawkins, J.W., Lonsdale, P., 1990. Fine-scale isotopic variation in Mariana Trough basalts: evidence for heterogeneity and a recycled component in backarc basin mantle. Earth Planet. Sci. Lett. 100, 251–264.

Volti, T., Gorbatov, A., Shiobara, H., Sugioka, H., Mochizuki, K., Kaneda, Y., 2006. Shear-wave splitting in the Mariana trough — a relation between back-arc spreading and mantle flow? Earth Planet. Sci. Lett. 244, 566–575.

Wade, J.A., Plank, T., Stern, R.J., Tollstrup, D.L., Gill, J.B., O'Leary, J.C., Eiler, J.M., Moore, R.B., Woodhead, J.D., Trusdell, F., Fischer, T.P., Hilton, D.R., 2005. The May 2003 eruption of Anatahan volcano, Mariana Islands: geochemical evolution of a silicic island-arc volcano. J. Volcanol. Geotherm. Res. 146, 139–170.

Wessel, P., Smith, W.H.F., 1991. Free software helps map and display data, Eos Trans. AGU, 72, 441, 445–446.

Wiens, D.A., Kelly, K.A., Plank, T., 2006. Mantle temperature variations beneath back-arc spreading centers inferred from seismology, petrology, and bathymetry. Earth Planet. Sci. Lett. 248, 30–42.

Woodhead, J.D., 1989. Geochemistry of the Mariana Arc (western Pacific): source composition and processes. Chem. Geol. 76, 1–24.

Yokoyama, T., Kobayashi, K., Kuritani, T., Nakamura, E., 2003. Mantle metasomatism and rapid ascent of slab components beneath island arcs: evidence from U-238–Th-230–Ra-226 disequilibria of Miyakejima volcano, Izu arc, Japan. J. Geophys. Res. 108. doi:10.1029/2002JB002103.

Yokoyama, T., Kuritani, T., Kobayashi, K., Nakamura, E., 2006. Geochemical evolution of a shallow magma plumbing system during the last 500 years, Miyakejima volcano, Japan: constraints from U-238–Th-230–Ra-226 systematics. Geochim. Cosmochim. Acta 70, 2885–2901.

Yoshizawa, K., Kennett, B.L.N., 2002a. Non-linear waveform inversion for surface waves with a neighbourhood algorithm — application to multimode dispersion measurements. Geophys. J. Int. 149, 118–133.

Yoshizawa, K., Kennett, B.L.N., 2002b. Determination of the influence zone for surface wave paths. Geophys. J. Int. 149, 440–453.

Yoshizawa, K., Kennett, B.L.N., 2004. Multimode surface wave tomography for the Australian region using a three-stage approach incorporating finite frequency effects. J. Geophys. Res. 109, B02310. doi:10.1029/2002JB002254.